

Communication

SOI-Based Multi-Channel AWG with Fiber Bragg Grating Sensing Interrogation System

Siming Weng ^{1,2} , Pei Yuan ^{1,2}, Wei Zhuang ^{1,2}, Dongliang Zhang ^{1,2}, Fei Luo ^{1,2} and Lianqing Zhu ^{1,2,*}

- ¹ Key Laboratory of the Ministry of Education for Optoelectronic Measurement Technology and Instrument, Beijing Information Science & Technology University, Beijing 100192, China; simingweng@163.com (S.W.); yuanpei@bistu.edu.cn (P.Y.); zhuangwei@bistu.edu.cn (W.Z.); zdl_photonics@bistu.edu.cn (D.Z.); feiluomail@gmail.com (F.L.)
- ² Beijing Laboratory of Optical Fiber Sensing and System, Beijing Information Science & Technology University, Beijing 100016, China
- * Correspondence: lqzhu_bistu@sina.com

Abstract: For the development of minimized and high-rate photonic-integrated fiber Bragg grating interrogation (FBGI) systems, arrayed waveguide grating (AWG) has been widely used as one of the critical components. In this paper, we present an 8-channel SOI-based AWG for a photonic integrated FBG interrogation microsystem. The channel spacing of the AWG is designed to be 3 nm to meet a high-dynamic-range demodulation requirement. The core size of the fabricated AWG is about $335 \times 335 \mu\text{m}^2$. The simulation results and experimental results are in high agreement, showing that AWG has a fine transmission spectrum with crosstalk below -16 dB, nonuniformity below 0.4 dB, insertion loss below -6.35 dB, 3 dB bandwidth about 1.3 nm and 10 dB bandwidth of 2.3 nm. The proposed AWG can be applied perfectly to the SOI-based AWG demodulation microsystem, exhibiting a large dynamic range of 1.2 nm, the resolution for measurements is 1.27 pm and a high accuracy of 20.6 pm.



Citation: Weng, S.; Yuan, P.; Zhuang, W.; Zhang, D.; Luo, F.; Zhu, L. SOI-Based Multi-Channel AWG with Fiber Bragg Grating Sensing Interrogation System. *Photonics* **2021**, *8*, 214. <https://doi.org/10.3390/photonics8060214>

Received: 12 May 2021
Accepted: 5 June 2021
Published: 10 June 2021

Publisher's Note: MDPI stays neutral with regard to jurisdictional claims in published maps and institutional affiliations.



Copyright: © 2021 by the authors. Licensee MDPI, Basel, Switzerland. This article is an open access article distributed under the terms and conditions of the Creative Commons Attribution (CC BY) license (<https://creativecommons.org/licenses/by/4.0/>).

Keywords: arrayed waveguide grating; silicon-on-insulator (SOI); fiber Bragg grating (FBG)

1. Introduction

To monitor the structural health and external environment of civil engineering, rail transit, aerospace, etc., and to ensure their safe operation, many kinds of sensors have been developed and widely used, one of which is the fiber Bragg grating (FBG) sensor [1–5]. FBG sensors are drawing more and more attention due to their obvious advantages over traditional electrical sensors such as low loss, high reliability, strong electromagnetic interference resistance, high temperature resistance, and simple structure [3,6,7]. The central wavelength of the FBG's reflected spectrum will shift with the variation of the environment, such as temperature, pressure, ultrasonic, etc. These physical parameters can be detected by demodulating the FBG wavelength. However, there are still some existing problems that are urgently required to be solved, especially the need for FBG interrogators (FBGIs) with small size, high rate, and high performance [8–10]. The existing commercial FBGIs based on discrete optoelectronic components, such as dynamic matched grating filters, tunable Fabry–Perot filters, CCDs, usually limit the development and application of FBG sensing technology because of their inferiorities in size and demodulation speed [4,11–14]. In recent years, AWG-based photonic-integrated FBGI systems have gained attention because of their advantages of a compact structure, energy efficiency, and the possibility to realize high-speed interrogation, because the interrogation rate of the FBGI system is only affected by photodetector (PD) response time and AD sampling rate. As it is limited by the output characteristics of AWG, the currently reported demodulation system based on AWG cannot achieve a high resolution and a total measurement range. For example, in 2014 [15], Gent university reported an AWG-based FBGI with a high dynamic range of

40 nm, whereas its resolution was only 5 pm; in 2017 [16], Tianjin polytechnic university reported an AWG-based FBGI with a high resolution of 1 pm and the dynamic range was not mentioned; in 2019 [17] University of Naples Federico II reported an AWG-based FBGI with a dynamic range of 0.8 nm without mentioning the resolution. Among all the material systems—including InP, silica, polymer, and silicon-on-insulator (SOI)—that can fabricate AWGs, the silicon-on-insulator (SOI) wafer with a top silicon layer and a buried SiO₂ layer is the most promising one to realize the monolithic or hybrid integration of passive and active optoelectronic devices. This can come with a low cost, as SOI is compatible with the complementary metal oxide semiconductor (CMOS) technology [7,18–23]. Additionally, an ultrasmall size of AWG can be achieved on an SOI-based platform because of its high relative refractive index difference between Si and SiO₂, which offers high light field confinement and allows small-size waveguides and small-radius bent waveguides. However, most reported AWGs nowadays are basically designed for the communication application, while in the FBG sensing system, AWG with high bandwidth is preferred to get a large interrogation dynamic range [24]. Thus, it is very crucial to design and fabricate a high-performance SOI-based AWG, which is applicable for FBGI system.

In this paper, we have fabricated several ultra-small AWGs with central wavelengths of 1550 nm and built an FBGI system with the AWGs embedded in. Due to AWG’s spectral characteristics, the wavelength resolution and measurement range, both of which are the AWG-based interrogator, are mutually constrained. To solve this problem, the performance of the interrogation system was analyzed with different diffraction orders (M) and different arrayed waveguide quantities (N). We have optimized the structure of AWG to make it more applicable for the FBGI system, which has high-bandwidth spectra by optimizing the diffraction order and arrayed waveguide quantities. We have tested the AWG’s central wavelength varying with temperature. The simulated and experimental analysis of the designed AWG is carried out from the aspects of spectral characteristics and interrogation performance.

2. Design and Simulation

The proposed AWG interrogation system consists of an amplified spontaneous emission (ASE) broadband light source, an optical circular, FBGs, an AWG, PDs, and a data processing circuit as shown in Figure 1 [24]. When the reflected light from the FBG transmits to AWG, the spectrum of FBG will overlap with the transmission spectra of AWG. P_i and P_{i+1} are the maximum two output light power values of the AWG, which are the convolutions of the FBG reflection spectrum and two adjacent channel transmission spectra of the AWG, respectively (see Figure 2). The central wavelength of FBG (λ_{FBG}) exhibits linear function with the logarithm of light power ratio of AWG’s two adjacent channels ($\ln \frac{P_{i+1}}{P_i}$), as shown in Equation (5). Employing Equation (5), the FBG wavelength can be interrogated by detecting P_i and P_{i+1} .

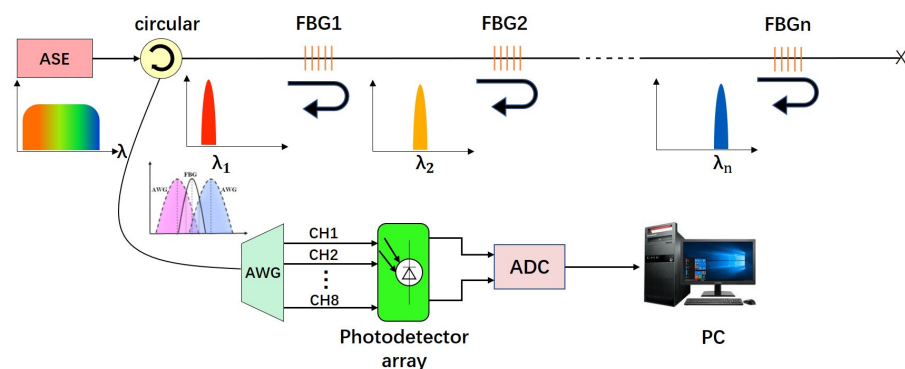


Figure 1. Schematic diagram of the AWG interrogation system.

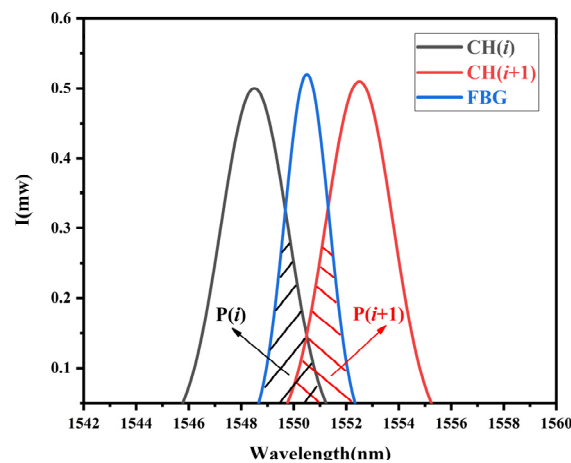


Figure 2. FBG spectra in pace with the spectrum from two AWG channels.

The transmission spectra of each channel of AWG can be assumed to be a Gaussian-like function, and the equation for the channel (i) of the AWG can be depicted as:

$$T_{AWG}(i, \lambda) = T_0 \exp \left\{ -4 \ln 2 \frac{(\lambda - \lambda_i)^2}{\Delta \lambda_i^2} \right\} \quad (1)$$

where T_0 is the normalization factor of AWG transmission spectrum; λ_i indicates the central wavelength of AWG Channel (i); $\Delta \lambda_i$ is the full width at half maximum (FWHM) of the AWG spectra.

Supposing the reflection spectrum of FBG is Gaussian, the reflection spectral equation of it will be:

$$R_{FBG}(\lambda) = R_0 \exp \left\{ -4 \ln 2 \frac{(\lambda - \lambda_{FBG})^2}{\Delta \lambda_{FBG}^2} \right\} \quad (2)$$

where R_0 is the normalization factor of FBG transmission spectrum; λ_{FBG} is the central wavelength of fiber Bragg grating (FBG); $\Delta \lambda_{FBG}$ is the full width at half maximum (FWHM) of the FBG spectrum.

The output optical power of AWG each channel is the integral of the light source power, FBG's reflection spectrum and AWG's transmission spectrum in the hole spectral region. As a result, the output optical power of AWG's channel (i) and channel ($i + 1$) is as follows:

$$P_i = (1 - L_i) \int_0^\infty I_s(\lambda) \cdot R_{FBG}(\lambda) \cdot T_{AWG}(i, \lambda) d\lambda \quad (3)$$

$$P_{i+1} = (1 - L_{i+1}) \int_0^\infty I_s(\lambda) \cdot R_{FBG}(\lambda) \cdot T_{AWG}(i + 1, \lambda) d\lambda \quad (4)$$

where L_i and L_{i+1} are the decay factors of channel (i) and channel ($i + 1$); $I_s(\lambda)$ is the optical power of the light source.

As we can recognize from Equations (1) and (2), the output optical power of AWG is closely related to the relative position of the peak wavelengths of AWG and FBG. Within a narrow wavelength range, the output optical power of broadband light source can be considered as a fixed value. Assuming that the channel spacing, full width at half maximum (FWHM), and the propagation coefficients of AWG each channel are identical, the relationship between the optical power ratio of AWG adjacent channels and FBG center wavelength is:

$$\ln \left(\frac{P_{i+1}}{P_i} \right) = \frac{8(\ln 2)\Delta \lambda}{\Delta \lambda_i^2 + \Delta \lambda_{FBG}^2} \lambda_{FBG} - \frac{4(\ln 2)(\lambda_{i+1}^2 + \lambda)}{\Delta \lambda_i^2 + \Delta \lambda_{FBG}^2} \quad (5)$$

Equation (5) shows the interrogation algorithm of FBG wavelength, which is that the logarithm of the output optical power ratio of AWG two adjacent channels has a

linear relationship with the reflected wavelength of FBG sensor. Thus, we only need to use photodetectors (PDs) to detect the AWG output optical power to demodulate the central wavelengths of FBGs.

The interrogation performance of the above FBGI system is closely related to the spectral characteristic of AWG, which is composed of input/output waveguides and two free propagation regions (FPRs) that are designed to provide focusing functionality, connected by an array of waveguides featuring a constant incremental optical path difference. The structural diagram of AWG is shown in Figure 3.

A beam of broad-band light transmitting through the input waveguide, diffracts in the first FPR and then is coupled into the arrayed waveguides. Before transmitting into the second FPR, the optical signals in adjacent arrayed waveguides have the same phase difference because of the same length difference (ΔL) in adjacent arrayed waveguides. The optical signals from different arrayed waveguides diffract and interfere with each other in the second FPR, and then the light of different wavelengths will focus on different location, finally outputting form different output waveguides.

We define Δx_0 as minimum separation output waveguides, ΔL as the path length difference of the adjacent arrayed waveguides, d as the minimum separation of arrayed waveguides, m as the diffraction order, λ and λ_0 as the wavelength in free-space, respectively, and $\Delta\lambda$ as the wavelength spacing. The relationships between these parameters are shown below.

$$\Delta L = \frac{m\lambda_0}{n_c} \tag{6}$$

$$\Delta\lambda = \frac{\Delta x_0 n_s d n_c}{R m n_g} \tag{7}$$

$$\text{FSR} = \frac{\lambda_0 n_c}{m n_g} \tag{8}$$

$$N \leq \frac{\text{FSR}}{\Delta\lambda} \tag{9}$$

where m is the diffraction order of the array, λ_0 is the center operating wavelength of AWG, n_c is the effective index of the arrayed waveguide, $\Delta\lambda$ is the spacing of the adjacent channel, FSR is the free spectral range of the device, n_s is the effective index of the slab waveguide, n_g is the group index, channel spacing, R is the diameter of the Rowland circle, and N is the maximal number of the output waveguides.

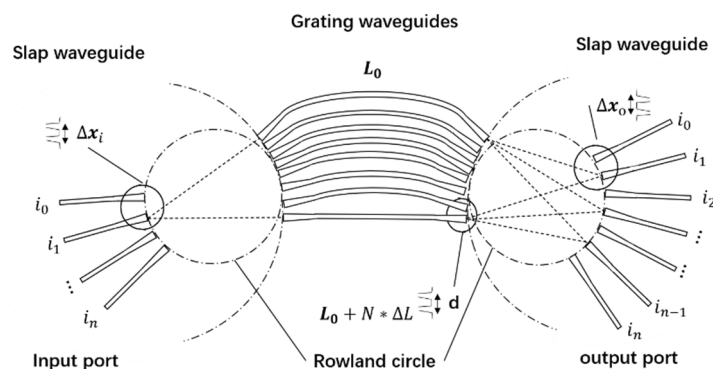


Figure 3. The structural diagram of AWG.

AWGs with different diffraction orders (m) and arrayed waveguide numbers (N) are designed to illustrate their impact on the spectral characteristic of AWG. Some parameters of AWG are revealed in Table 1. Figures 4 and 5 respectively shows the variation of transmission spectrum of two adjacent AWG channels under different diffraction orders and different array waveguide numbers. The principle of the demodulation system is that the central wavelength of the fiber Bragg grating (λ_{FBG}) is placed between the central

wavelength of the adjacent channel of the AWG, if central wavelength of the Bragg shifts, the power distribution in each of the adjacent channels will change. Therefore, when the AWG is used for demodulation, its transmission spectrum needs to have small crosstalk and large overlap range to improve the measurement range and accuracy of the system. If the crosstalk between the adjacent AWG channels gets smaller and the overlap area becomes larger, the demodulation performance of the system will be better. From Figure 4, we can see that the overlap area and crosstalk of the adjacent channel become smaller when the diffraction order (M) and number of the arrayed waveguides (N) get higher. Through the simulation we find that when $M = 20$ and $N = 25$, the transmission spectrum of AWG has relatively small crosstalk and large overlap range at the same time, which is suitable for the demodulation system. Some parameters of the AWGs are shown in Table 1.

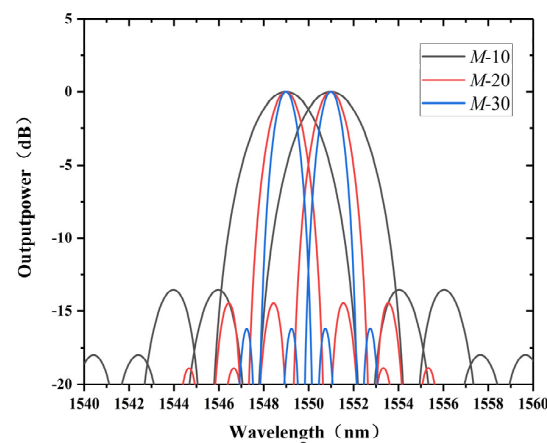


Figure 4. Transmission spectra of adjacent AWG channels under different diffraction orders (M).

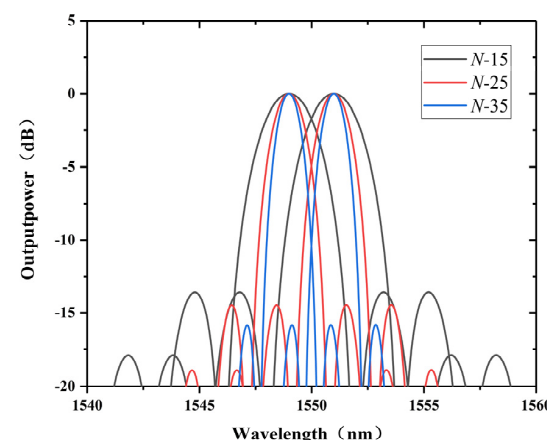


Figure 5. Transmission spectra of adjacent AWG channels under different arrayed waveguide quantities (N).

Table 1. Parameters of designed SOI-based multi-channel AWG (8 × 8).

Items	SOI-Based AWG (8 × 8)
Diffraction order	20
ΔL (μm)	30
Number of arrayed waveguides	25
Free spectral range (nm)	60
Width of the waveguide (μm)	0.5
Channel spacing (nm)	3

With the optimized parameters of diffraction order and arrayed waveguide number, the spectrum of AWG is presented in Figure 6, from which we can conclude that the AWG has good transform spectrum with central channel loss of -3.18 dB, nonuniformity below 0.4 dB, crosstalk below -16 dB, and 3 dB bandwidth about 1.3 nm.

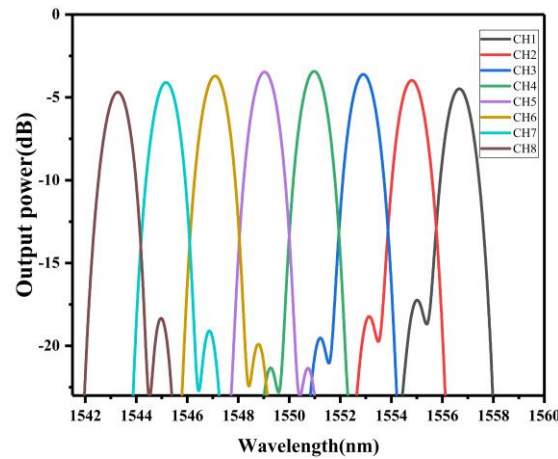


Figure 6. Simulation results of saddle-shaped 8×8 AWG.

3. Device Structure and Experiment

Our SOI-based multi-channel AWG is fabricated on silicon-on-insulator (SOI) wafer with a top silicon layer, and a buried SiO_2 layer. Figure 7 is the microscope graphs of fabricated 8×8 AWG. Figure 7a shows the complete structure of the AWG, Figure 7b shows the output waveguides, Figure 7c shows the arrayed waveguides, Figure 7d shows the input waveguides, Figure 7e shows the grating couplers, and Figure 7f shows the bi-level-tapers which have been proven to be effective in reducing the crosstalk caused by optical field coupling while maintaining a high mode converting efficiency [16]. The core size of the fabricated AWG is $335 \times 335 \mu\text{m}^2$.

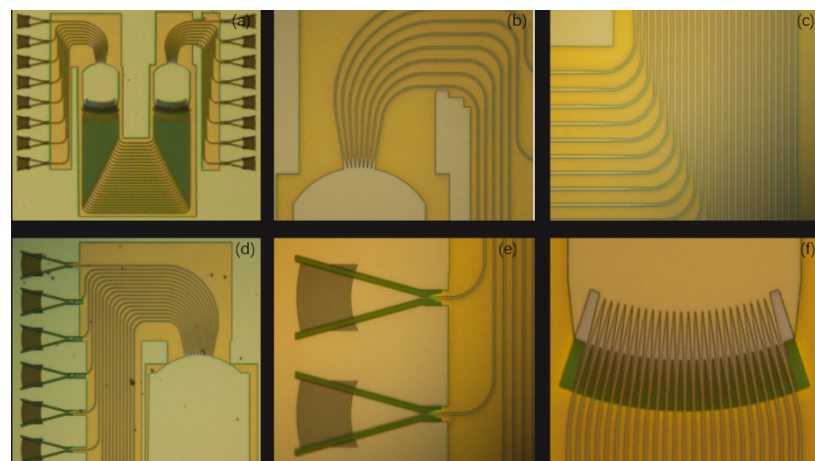


Figure 7. Microscope photo of (a) fabricated 8×8 AWG; (b) output waveguides; (c) arrayed waveguides; (d) input waveguides; (e) grating coupler; (f) the tapers between input/output waveguides and FPR.

The n_c of AWG is affected by temperature. The spectral characteristic, namely the peak wavelength of AWG is temperature related, which is caused by the dependence of n_c on the temperature. Relationship between each channel’s central wavelength and temperature is as follows:

$$\lambda_i(T) = \lambda_i(T_0) + \frac{dn_c}{dT} \times \frac{\Delta L}{m} \times \Delta T \tag{10}$$

where λ_i is the central wavelength of each channel’s transmission spectrum, T is the temperature of AWG, T_0 is the original temperature of AWG and ΔT is the value of T and T_0 . Figure 8 shows the test result of AWG’s central wavelength varying with temperature. Figure 8a is the transmission spectra at different temperatures of the fifth output channel (CH5) of the AWG and Figure 8b is the relationship between the central wavelength of CH5 and temperature of AWG.

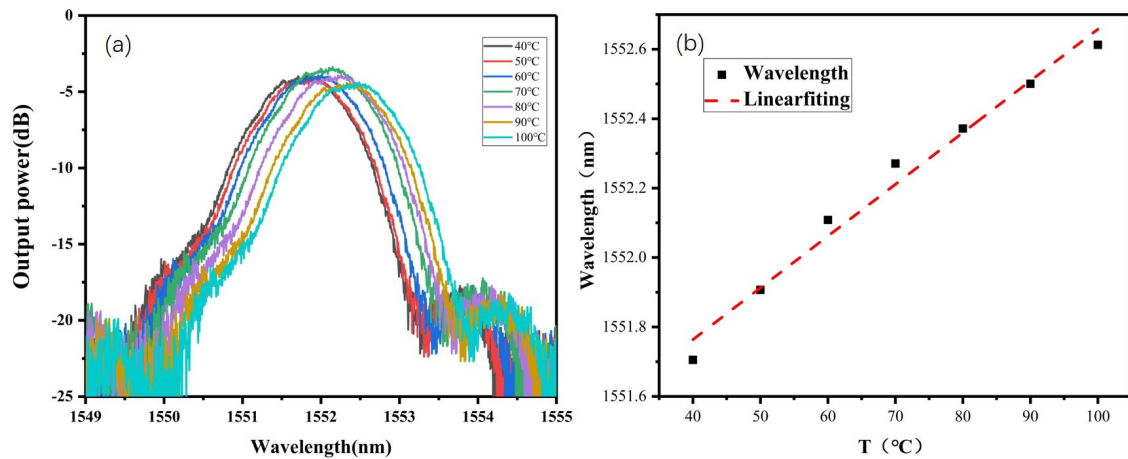


Figure 8. (a) the transmission spectra at different temperatures of the fifth output channel (CH5) of the AWG. (b) the relationship between the central wavelength of CH5 and temperature of AWG.

We can see that the output characteristics of AWG are influenced by temperature and that the central wavelength of each channel’s output spectrum will drift with temperature. This phenomenon will reduce the accuracy of the interrogation system, so we did experiments in the ultra-clean room with a constant temperature.

Figure 9 shows the testing system for the spectra measurement of the fabricated AWG. The optical signal from an ASE C-band source is coupled into AWG’s input waveguide on the 6-axis adjustment platform through a single-mode lens fiber. Afterwards the light from AWG’s output waveguide is coupled into a 1 × 2 splitter connected to an optical spectral analyzer and a power meter, respectively. The optical signal that travels through the power meter is converted into a digital signal which can be recognized by the computer that is an important reference for using the computer to control the motion controller, which is used to implement the rigid control of the 6-axis adjustment platform.

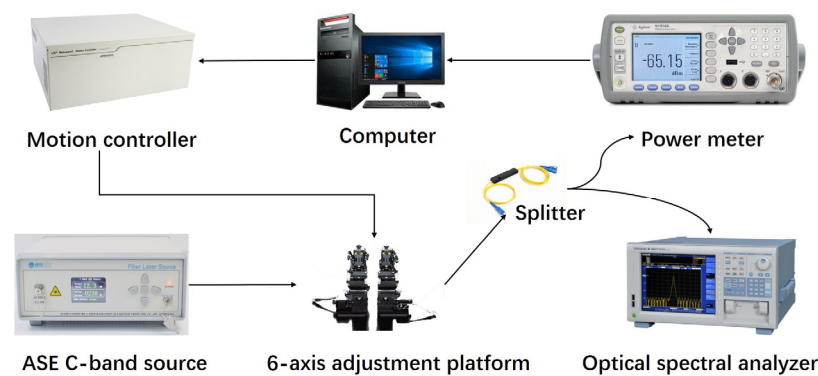


Figure 9. Testing system for the spectrum measurement of the fabricated AWG.

The transmission spectrum shows that the fabricated AWG exhibits a central channel loss of -4.35 dB, loss uniform of 0.8 dB, and crosstalk level of -15.4 dB, as shown in Figure 10. The amplitude of transmission spectrum of each channel is not uniform which is partially caused by the difference from the coupling loss of each channel of AWG.

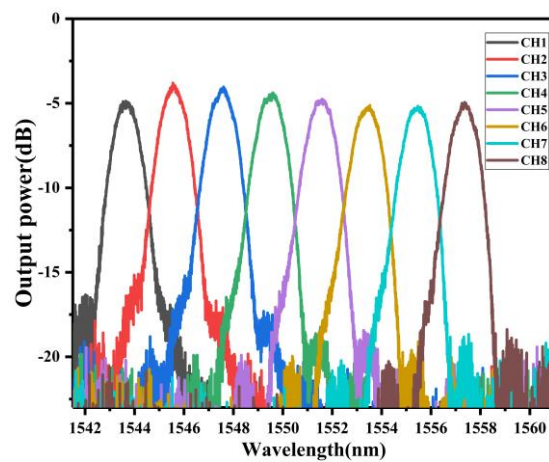


Figure 10. Experiment results of saddle-shaped 8 × 8 AWG.

Due to the limitation of inductively coupled plasma technology, the produced waveguide will produce manufacturing errors. Thus, there are differences between the simulation and experimental results. Nevertheless, the transmission spectrum of the device has reached the expected performance in terms of crosstalk, nonuniformity and insertion loss (see Table 2).

Table 2. Comparison of the simulation and experiment results.

	Crosstalk	Central Channel Loss	Nonuniformity
Simulation results	−16 dB	−3.18 dB	0.4 dB
Experiment results	−15.4 dB	−4.35 dB	0.8 dB

Figure 11 shows the testing system for the interrogation performance measurement of the fabricated AWG. The broadband light emitted by the ASE is coupled through a single-mode fiber into the fiber Bragg grating, which is located on the temperature control table. The light reflected from the FBG pass through the optical circular and then transmits to AWG which is placed on a 6-axis adjustment platform. Then optical signal from AWG’s output waveguide travels into the power meter. Finally, the optical signal is converted into electrical signal by optical power meter. The motion controller is used to adjust the position of the output coupling fiber to collect the maximum optical power of each output channels.

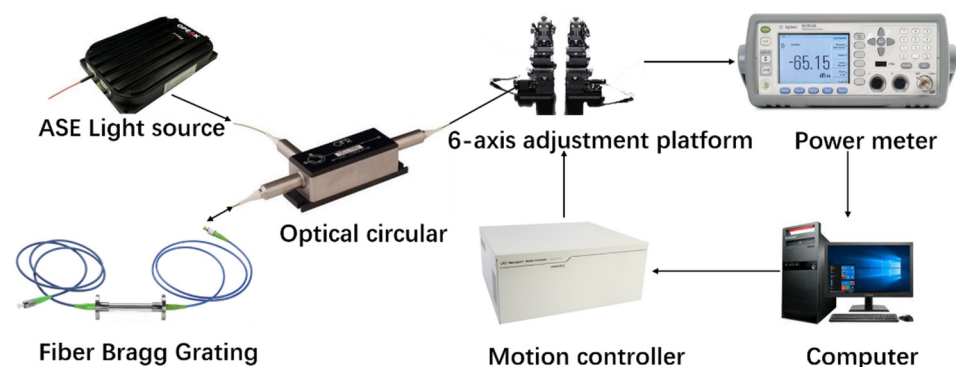


Figure 11. Testing system for the interrogation performance measurement of the fabricated AWG.

Based on Equation (5), we experimentally analyzed the relationship between the logarithm of the output optical power ratio ($\ln(\frac{P_{i+1}}{P_i})$) of AWG adjacent channels (AWG channel 1 and 2 and channel 7 and 8, respectively, as shown in Figure 12a,b, and the peak wavelength of FBG. The relationship between the logarithm of the optical power ratio and

the peak wavelength of the FBG is obtained by linear fitting. The root mean square (RMS) of the fitting line and the experimental data is 20.9 pm, so that the measured wavelength precision of the AWG based FBGI system is 20.9 pm. The wavelength sensitivity of each FBG is between 1.3 and 1.75 dB/nm, which is relatively high and promising to get a high wavelength resolution. The demodulating range in this paper is about 1 nm, less than the channel spacing of AWG, because the adjacent channel crosstalk of AWG is not negative infinite. The experimental results in this paper show that the AWG based FBG interrogation system is an excellent choice for fiber Bragg grating sensing systems.

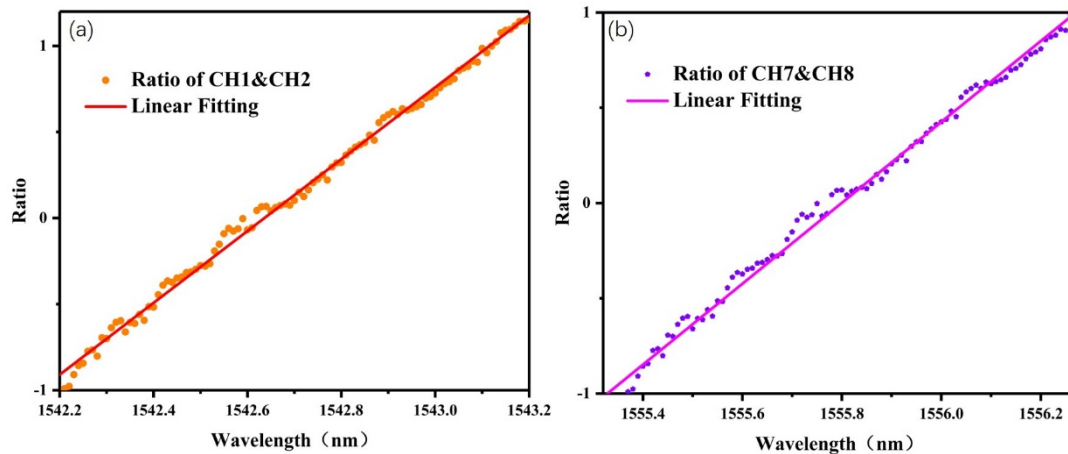


Figure 12. (a) The logarithm of the output optical power ratio ($\ln(\frac{P_{i+1}}{P_i})$) of AWG adjacent channels (channel 7 and 8). (b) The logarithm of the output optical power ratio ($\ln(\frac{P_{i+1}}{P_i})$) of AWG adjacent channels (channel 1 and 2).

We made a comparison of proposed interrogation system and the interrogation system of recent studies [16,24] (see Table 3). The proposed interrogation system has good performance in dynamic range, resolution and accuracy.

Table 3. Comparison of recent studies.

Interrogation Systems of Resent Studies	Dynamic Range	Resolution	Accuracy
Our proposed interrogation system	1 nm	1.2 pm	20.6 pm
Interrogation system [16]	0.4 nm	1 pm	10 pm
Interrogation system [24]	unknown	1 pm	40–60 pm

4. Conclusions

An SOI-based multi-channel AWG was designed, fabricated, and tested in this article. The core sizes of the proposed AWG are smaller than $335 \times 335 \mu\text{m}^2$. In the simulation results that basically correspond to the experiment, the AWG has a fine transmission spectrum with crosstalk below -16 dB, central channel loss of -3.18 dB, 10 dB bandwidth of 2.3 nm, 3 dB bandwidth about 1.3 nm, the resolution for measurements is 1.27 pm with a wavelength accuracy of roughly 20.6 pm. The experiments in this paper aim toward the optimization of AWGs used for FBG interrogation systems. The experimental results show that the AWG based FBG interrogation system has a great potential for a good-performance and is an excellent choice for fiber Bragg grating sensing systems.

Author Contributions: S.W. (the leading author of the paper) performed the numerical simulations to evaluate the device performances, carried out the experimental tests, performed the data analyses and wrote the manuscript; P.Y. designed the AWG device and provided valuable advice for writing the article; W.Z. contributed significantly to the data processing; D.Z. coordinated the structure of this work; F.L. played an important role in performing the analysis with constructive discussions; L.Z.

provided experimental sites and instruments and put forward guiding suggestions for the project. All authors have read and agreed to the published version of the manuscript.

Funding: This research was funded by 111 project, grant number D17021.

Acknowledgments: This work has been supported by 111 project (D17021), and the Opened Fund of the State Key Laboratory of Integrated Optoelectronics (No. IOSKL2020KF21). Thank the Henan Shijia Photons Technology Co (Henan China), Ltd. for the support of AWG devices.

Conflicts of Interest: The authors declare no conflict of interest.

References

1. Wang, T.; Liu, K.; Jiang, J.; Xue, M.; Chang, P. Temperature-insensitive refractive index sensor based on tilted moiré FBG with high resolution. *Opt. Express* **2017**, *25*, 14900–14909. [[CrossRef](#)]
2. Culshaw, B.; Kersey, A. Kersey, Fiber-optic sensing: A historical perspective. *J. Lightwave Technol.* **2008**, *26*, 1064–1078. [[CrossRef](#)]
3. Hill, K.; Meltz, G. Fiber Bragg grating technology fundamentals and overview. *J. Light. Technol.* **1997**, *15*, 1263–1276. [[CrossRef](#)]
4. Diaz, C.A.R.; Leal-Junior, A.G.; Avellar, L.; Antunes, P.F.C.; Pontes, M.J.; Marques, C.A.; Frizera, A.; Ribeiro, M.R.N. Perrogator: A Portable Energy-Efficient Interrogator for Dynamic Monitoring of Wavelength-Based Sensors in Wearable Applications. *Sensors* **2019**, *19*, 2962. [[CrossRef](#)]
5. Leal-Junior, A.G.; Diaz, C.A.; Avellar, L.; Pontes, M.J.; Marques, C.; Frizera, A. Polymer Optical Fiber Sensors in Healthcare Applications: A Comprehensive Review. *Sensors* **2019**, *19*, 3156. [[CrossRef](#)]
6. González-Vila, Á.; Kinet, D.; Mégret, P.; Caucheteur, C. Narrowband interrogation of plasmonic optical fiber biosensors based on spectral combs. *Opt. Laser Technol.* **2017**, *96*, 141–146. [[CrossRef](#)]
7. Cheben, P.; Post, E.; Janz, S.; Albert, J.; Laronche, A.; Schmid, J.H.; Xu, D.-X.; Lamontagne, B.; Lapointe, J.; Delâge, A.; et al. Tilted fiber Bragg grating sensor interrogation system using a high-resolution silicon-on-insulator arrayed waveguide grating. *Opt. Lett.* **2008**, *33*, 2647–2649. [[CrossRef](#)]
8. Pei, Y.; Yuanda, W.; Yue, W.; An, J.; Hu, X. Monolithic integration of a 16-channel VMUX on SOI platform. *J. Semicond.* **2015**, *36*, 084005.
9. Li, H.; Gao, W.; Li, E.; Tang, C. Investigation of Ultrasmall $1 \times N$ AWG for SOI-Based AWG Demodulation Integration Microsystem. *IEEE Photon. J.* **2015**, *7*, 1–7. [[CrossRef](#)]
10. Jiang, Y.; Ding, W.; Liang, P.; Fu, L.; Wang, C. Phase-Shifted White-Light Interferometry for the Absolute Measurement of Fiber Optic Mach–Zehnder Interferometers. *J. Light. Technol.* **2010**, *28*, 3294–3299. [[CrossRef](#)]
11. Zi-Jun, B.; Jian-Lin, Z.; En-Pu, L.; Wang-Min, Z.; Bi-Qiang, J.; Quan-Chao, L.; Zhen-Long, C. Optimization of Dynamic Matched Grating Filtering Demodulation Driven by Piezoelectric Ceramic. *Acta Photonica Sin.* **2010**, *39*, 243. [[CrossRef](#)]
12. Harish, A.V.; Varghese, B.; Rao, B.; Balasubramaniam, K.; Srinivasan, B. Dynamic interrogator for elastic wave sensing using Fabry Perot filters based on fiber Bragg gratings. *Ultrasonics* **2015**, *60*, 103–108. [[CrossRef](#)]
13. Qian, S.-B.; Xiang, F.-Y.; Zhu, L.-Y.; Dai, Z.-B.; He, J.-J.; Yuan, J.-Z. A New CCD Photometric Investigation of the Short-Period Close Binary AP Leonis. *Astron. J.* **2006**, *133*, 357–363. [[CrossRef](#)]
14. Diaz, C.A.; Leitão, C.; Marques, C.A.; Domingues, M.F.; Alberto, N.; Pontes, M.J.; Frizera, A.; Ribeiro, M.; André, P.S.; Antunes, P.F.J.S. Low-cost interrogation technique for dynamic measurements with FBG-based devices. *Sensors* **2017**, *17*, 2414. [[CrossRef](#)] [[PubMed](#)]
15. Trita, A.; Vickers, G.; Mayordomo, I.; van Thourhout, D.; Vermeiren, J. Design, integration, and testing of a compact FBG interrogator, based on an AWG spectrometer. In Proceedings of the Silicon Photonics and Photonic Integrated Circuits IV, Brussels, Belgium, 13–17 April 2014. [[CrossRef](#)]
16. Li, H.; Ma, X.; Cui, B.; Wang, Y.; Zhang, C.; Zhao, J.; Zhang, Z.; Tang, C.; Li, E. Chip-scale demonstration of hybrid III-V/silicon photonic integration for an FBG interrogator. *Optica* **2017**, *4*, 692–700. [[CrossRef](#)]
17. Marrazzo, V.R.; Riccio, M.; Maresca, L.; Irace, A.; Breglio, G. Wide Range AWG-Based FBG Interrogation System with Improved Sensitivity. In Proceedings of the 2019 15th Conference on Ph. D Research in Microelectronics and Electronics (PRIME), Lausanne, Switzerland, 15–18 July 2019; pp. 149–152.
18. Stoll, A.; Zhang, Z.; Haynes, R.; Roth, M. High-Resolution Arrayed-Waveguide-Gratings in Astronomy: Design and Fabrication Challenges. *Photonics* **2017**, *4*, 30. [[CrossRef](#)]
19. Yebo, N.A.; Bogaerts, W.; Hens, Z.; Baets, R. On-Chip Arrayed Waveguide Grating Interrogated Silicon-on-Insulator Microring Resonator-Based Gas Sensor. *IEEE Photon. Technol. Lett.* **2011**, *23*, 1505–1507. [[CrossRef](#)]
20. Pustakhod, D.; Kleijn, E.; Williams, K.; Leijtens, X. High-Resolution AWG-Based Fiber Bragg Grating Interrogator. *IEEE Photon. Technol. Lett.* **2016**, *28*, 2203–2206. [[CrossRef](#)]
21. Hibino, Y. Recent advances in high-density and large-scale AWG multi/demultiplexers with higher index-contrast silica-based PLCs. *IEEE J. Sel. Top. Quantum Electron.* **2002**, *8*, 1090–1101. [[CrossRef](#)]
22. Su, H.; Huang, X.G. A novel fiber Bragg grating interrogating sensor system based on AWG demultiplexing. *Opt. Commun.* **2007**, *275*, 196–200. [[CrossRef](#)]

-
23. Ruocco, A.; Van Thourhout, D.; Bogaerts, W. Silicon Photonic Spectrometer for Accurate Peak Detection Using the Vernier Effect and Time-Domain Multiplexing. *J. Light. Technol.* **2014**, *32*, 3351–3357. [[CrossRef](#)]
 24. Li, H.; Zhou, W.; Liu, Y.; Dong, X.; Zhang, C.; Miao, C.; Zhang, M.; Li, E.; Tang, C. Preliminary investigation of an SOI-based arrayed waveguide grating demodulation integration microsystem. *Sci. Rep.* **2014**, *4*, 1–6.